NRC·CNRC

NRC Publications Archive
Archives des publications du CNRC

A probabilistic high-pressure zone model for local and global loads during ice-structure interactions

Taylor, Rocky S.; Richard, Martin; Hossain, Ridwan

This publication could be one of several versions: author's original, accepted manuscript or the publisher's version. / La version de cette publication peut être l'une des suivantes : la version prépublication de l'auteur, la version acceptée du manuscrit ou la version de l'éditeur.
For the publisher's version, please access the DOI link below./ Pour consulter la version de l'éditeur, utilisez le lien DOI ci-dessous.

Publisher's version / Version de l'éditeur:
https://doi.org/10.1115/1.4042386
Journal of Offshore Mechanics and Arctic Engineering, 141, 5, 2019-02-15

NRC Publications Archive Record / Notice des Archives des publications du CNRC :
https://nrc-publications.canada.ca/eng/view/object/?id=f7249c88-fb82-45ac-81c0-5cf1667d69e6
https://publications-cnrc.canada.ca/fra/voir/objet/?id=f7249c88-fb82-45ac-81c0-5cf1667d69e6

Access and use of this website and the material on it are subject to the Terms and Conditions set forth at
https://nrc-publications.canada.ca/eng/copyright
READ THESE TERMS AND CONDITIONS CAREFULLY BEFORE USING THIS WEBSITE.

L'accès à ce site Web et l'utilisation de son contenu sont assujettis aux conditions présentées dans le site
https://publications-cnrc.canada.ca/fra/droits
LISEZ CES CONDITIONS ATTENTIVEMENT AVANT D'UTILISER CE SITE WEB.

Questions? Contact the NRC Publications Archive team at PublicationsArchive-ArchivesPublications@nrc-cnrc.gc.ca. If you wish to email the authors directly, please see the first page of the publication for their contact information.

Vous avez des questions? Nous pouvons vous aider. Pour communiquer directement avec un auteur, consultez la première page de la revue dans laquelle son article a été publié afin de trouver ses coordonnées. Si vous n'arrivez pas à les repérer, communiquez avec nous à PublicationsArchive-ArchivesPublications@nrc-cnrc.gc.ca.

National Research Council Canada | Conseil national de recherches Canada

Canada

A Probabilistic High-Pressure Zone Model for Local and Global Loads During Ice-Structure Interactions

Rocky S. Taylor
Assistant Professor
Department of Mechanical Engineering,
Memorial University of Newfoundland,
St. John's, NL A1C 5S7, Canada
e-mail: rstaylor@mun.ca

Martin Richard
National Research Council Canada (NRC),
1 Arctic Avenue,
St. John's, NL A1B 3T5, Canada;
Adjunct Professor
Department of Civil Engineering,
Memorial University of Newfoundland,
St. John's, NL A1C 5S7, Canada
e-mail: martin.richard@nrc-cnrc.gc.ca

Ridwan Hossain[1]
Department of Mechanical Engineering,
Memorial University of Newfoundland,
St. John's, NL A1C 5S7, Canada
e-mail: rbh546@mun.ca

For temperate ice regions, guidance provided by current design codes regarding ice load estimation for thin ice is unclear, particularly for local pressure estimation. This is in part due to the broader issue of having different recommended approaches for estimating local, global, and dynamic ice loads during level ice interactions with a given structure based on region, scenario type, and a variety of other conditions. It is essential from a design perspective that these three scenarios each be evaluated using appropriate definitions for local design areas, global interaction area, and other structural details. However, the need for use of different modeling approaches for ice loads associated with each of these scenarios is not based on ice mechanics but rather has largely evolved as a result of complexities in developing physics-based models of ice failure in combination with the need to achieve safe designs in the face of limited full-scale data and the need for implementation in a probabilistic framework that can be used for risk-based design assessments. During a given interaction, the ice is the same regardless of the design task at hand. In this paper, a new approach is proposed based on a probabilistic framework for modeling loads from individual high-pressure zones acting on local and global areas. The analysis presented herein considers the case of thin, first-year sea ice interacting with a bottom-founded structure based on an empirical high-pressure zone model derived from field measurements. Initial results indicate that this approach is promising for modeling local and global pressures.
[DOI: 10.1115/1.4042386]

1 Introduction

Modeling extreme ice actions is essential in the design of ships and offshore structures for ice environments. During the compressive failure of ice against a vertical-walled structure, global and local pressures associated with ice crushing failure have important implications for design. Widely accepted trends of decreasing ice pressure with increasing area have been incorporated into design codes such as ISO 19906 [1] and considerable effort has been placed on reducing uncertainty associated with such pressure–area relationships [2–6]. While such pressure–area relationships provide valuable guidance, many approaches do not explicitly account for statistical exposure effects and rather assume that extreme value for design can be modeled from these data as the mean peak pressure plus three standard deviations. Such an approach assumes normally distributed residuals and moreover does not allow the analyst to account for differences between structures experiencing very infrequent interactions, which would be expected to experience smaller extreme loads than those exposed to many annual interactions.

Various probabilistic models of ice pressure behavior have been developed to model loads during interactions between ships and offshore structures with ice (e.g., see Refs. [7–19]). Many of these approaches treat ice loads as a Poisson-type process and rely on statistical information or empirical relations extracted from force–time series measurements from instrumented ice load panels with fixed area. Ice failure is a complex process and the direct use of field data as a basis for design load estimation continues to be a necessity in ensuring safe, economical designs.

Probabilistic methods for extreme ice pressure analysis, such as the event-maximum method, also show very clear scale effects but provide an approach in which design exposure and exceedance probability are explicitly accounted for (e.g., see Refs. [8] and [13]). Such an approach allows the designer to more clearly link estimated design loads with target safety levels based on the operational profile of the vessel or structure. Such probabilistic methods are well suited to the analysis of local panel pressure data, where ice loads are measured over structural panels of fixed areas. High-resolution tactile pressure sensor data, such as that made available by the Japan Ocean Industries Association (JOIA) medium-scale field indentation program, have provided opportunities to study and model pressures at the scale of the fundamental element of compressive ice failure: the high-pressure zone.

High-pressure zones (*hpz*s) are regions of localized contact through which the ice transmits intense local pressures to the structure during an ice–structure interaction [20,21]. Individual *hpz*s have high temporal and spatial variability, and collectively, all *hpz*s present during an interaction are responsible for the majority of loads transmitted to the structure. For structures interacting with level sea ice, linear patterns of *hpz*s or "line-loads" are typically observed across the width of the interaction area [22–25]. The ice feature geometry plays an important role in the shape of the contact pressure distribution, as was recognized in the geometrical model of Spencer and Masterson [26]. For the case of level ice interactions, the shape of the spatial distribution of *hpz*s is influenced by the occurrence of spalling fractures which extend to the top and bottom surfaces of the ice sheet and tend to concentrate *hpz*s near the center of thickness of the ice sheet. Observations from the JOIA tactile pressure sensor dataset suggest that the total contact area (combined area of all *hpz*s) during

[1]Corresponding author.

Contributed by the Ocean, Offshore, and Arctic Engineering Division of ASME for publication in the Journal of Offshore Mechanics and Arctic Engineering. Manuscript received June 20, 2018; final manuscript received December 17, 2018; published online February 15, 2019. Assoc. Editor: Zhen Gao.

Copyright © 2019 by ASME; reuse license CC-BY 4.0

Downloaded From: https://offshoremechanics.asmedigitalcollection.asme.org on 05/03/2019 Terms of Use: http://www.asme.org/about-asme/terms-of-use

crushing events is on average only about 10% of the nominal interaction area [24,25].

During ship–ice ramming events with multiyear ice, pressures as high as 70 MPa have been measured [27]. Similarly, very intense local pressures have been measured during medium-scale indentation tests on multiyear sea ice and pressures as high as 60 MPa [28] and 80 MPa [20] have been reported. From small-scale indentation tests on polycrystalline freshwater ice at −10 °C, pressures greater than 100 MPa have been reported for areas of a few squaremillimeters, while pressures on the order of 35 MPa on areas of a few hundred squaremillimeters have been reported [29,30]. Given the important role of high-pressure zones in determining the loads transmitted to a structure during an ice–structure interaction, understanding the nature of *hpz*s and associated mechanics is key to developing improved models of local and global ice pressures.

While panel measurements provide valuable data for ice load modeling, they typically do not provide adequate resolution to track the spatial and temporal evolution of individual *hpz*s. Tactile pressure sensor data, such as those available from the JOIA medium-scale field indentation tests, provide detailed information about pressure distributions at a higher resolution than previously available. These data provide valuable insights into the nature of compressive failure processes for thin first-year sea ice [23,31–35].

Tactile pressure sensor data also highlight the complexity of the load limiting processes present during an ice–structure interaction. Throughout a given crushing event, the loads acting on a given region may be attributed to either a single *hpz*, a partial *hpz*, or multiple *hpz*s. If one has sufficient full-scale panel data to confidently represent all loading conditions encountered by a structure over its design life, this high degree of detail may be considered as unnecessary since the designer is primarily concerned with the extreme level of load acting over the specified area (local or global). However, when designing for conditions for which such data are unavailable, when there is significant uncertainty regarding interpretation of available data, or in developing next generation dynamic ice–structure interaction models, the behavior of *hpz*s is critically important. In such cases, understanding the details of ice failure processes, *hpz* behavior, and associated mechanics provide an additional layer of information to help guide design load estimation.

Several models have been developed that utilize inferences about *hpz*s from local panel pressure data, see, for example, Refs. [1], [10], [11], [16], and [21]. In many of these models, pressure is modeled as a combination of *hpz* pressures and a low background pressure, with estimates of pressure contributions being inferred from local pressure panel data. For many datasets, the size of the instrumented panels provides adequate resolution to allow one to estimate the area of the loaded region but does not provide adequate detail to track the true contact areas of individual *hpz*s within that region. To identify, track, and extract data for individual *hpz*s from tactile pressure sensor data, a new algorithm has been developed [36]. Using this algorithm, an analysis of the JOIA dataset has been undertaken and a database of "empirical *hpz*s" has been compiled to help characterize *hpz* attributes and associated load limiting mechanisms.

To provide insights into the behavior of *hpz*s during the compressive failure of first-year sea ice, a detailed analysis of the tactile pressure data from the JOIA program has been undertaken and a new ice load model based on extracted *hpz* data has been developed. In the present paper, a description of the data analysis and a summary of results are provided. A new ice load model based on the ensemble behavior of empirical *hpz*s has been developed and implemented to simulate level ice loads for interactions between a structure and thin first-year sea ice. Results obtained using this model are compared with results from existing local and global ice pressure models.

2 Methodology

As illustrated in Fig. 1, the methodological framework employed in the present work is comprised of three main steps: (1) analysis of data, (2) statistical *hpz* characterization, and (3) design load estimation. These are described below.

2.1 Analysis of Data

2.1.1 Experimental and Full-Scale Data. Data considered in the present analysis were obtained from indentation tests conducted on thin, first-year sea ice during the medium-scale field indentation test program carried out by the JOIA. Between 1996 and 2000, more than 30 field indentation experiments were carried out in the harbor of Notoro Lagoon in Hokkaido, Japan (44^{o}05′N, 144^{o}10′E). The field indentation apparatus consisted of a large mobile test frame that was suspended from the side of the main dock and which could be moved using a 65-ton mobile crane to allow the indenter to be placed at specified locations along the dock [23]. For test data considered in the present work, ice conditions consisted of brackish first-year sea ice, with some snow ice and an average ice thickness on the order of 30 cm. During this program, the mean air temperature was about −3 °C and the indentation rate, which was controlled by a servo-controlled hydraulic system, varied between 0.3 cm/s and 3 cm/s. Details of the ice conditions and the physical and mechanical properties of the ice during the program are detailed by Kamio et al. [33]. The indenter structure consisted of an instrumented beam (40 cm deep × 150 cm wide) fitted with 15 contiguous 10 cm wide load panels, which for many experiments were also instrumented with

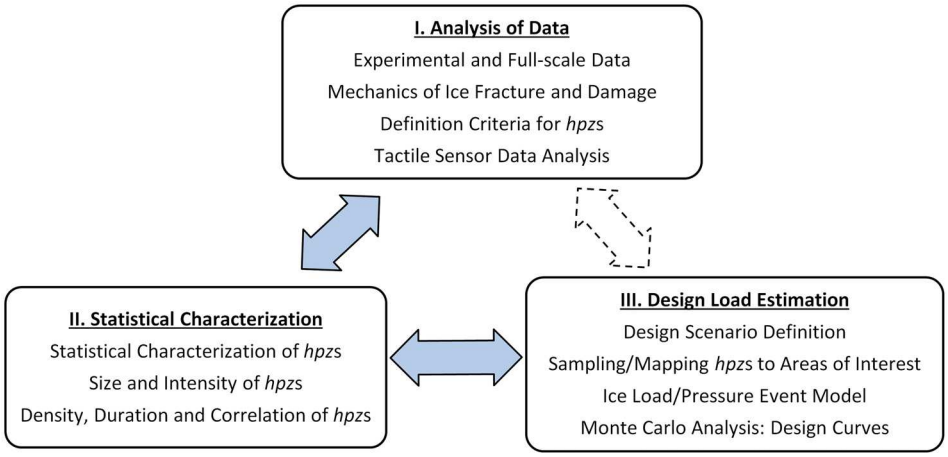

Fig. 1 Ice load modeling framework and approach for *hpz*-based model development

Downloaded From: https://offshoremechanics.asmedigitalcollection.asme.org on 05/03/2019 Terms of Use: http://www.asme.org/about-asme/terms-of-use

Tekscan tactile pressure sensors. The tactile pressure sensors used in test events considered in the present work consist of a 44 element high by 176 element wide array, in which each sensor element was 5.1994 mm × 5.1994 mm (27.0322 mm^2) and covered a 90 cm wide central region of the beam. Additional details of the JOIA program have been published by several authors [23,31,33–35,37].

2.1.2 Tactile Data Visualization and Extraction of Individual High-Pressure Zones. To facilitate easier processing, filtering, analysis, and interpretation of the raw JOIA data, a set of numerical tools and a graphical user interface (GUI) were developed in MATLAB. This work included an overall assessment of the dataset to examine general observations of ice failure behavior under different loading conditions. Sample data for Test 980126-1 plotted using the GUI developed for analyzing these data are shown in Fig. 2.

From an initial analysis of the tactile sensor data, it was evident that there are regions of surrounding background pressure, such as the regions shown in blue in Fig. 2 (for interpretation of the color, the reader is referred to the web version of the article), which can make it difficult to discriminate between contact areas associated with individual *hpz*s. To address this issue, several different techniques for identifying and delimiting *hpz*s have been explored. The selected technique was based on a combination of a threshold-based contact area definition and an *hpz* centroid tracking algorithm. For each time-step, contour lines corresponding to regions defined by areas having pressures above a specified threshold pressure were extracted from the tactile sensor data. To track the *hpz* evolution in time, it was assumed that if the centroid of a given *hpz* area did not shift by a distance of more than half the area width during subsequent time steps, then these areas could be assumed to correspond to the same *hpz*. For the purpose of this calculation, the width of each *hpz* was defined for each time-step as the difference between the maximum and minimum horizontal extents of the corresponding *hpz* contour line. Shifts in the centroid that were greater than half the *hpz* width were taken as an indicator of the "death" of one *hpz* and if a nearby *hpz* area was present in the time steps following a death, this was interpreted as the "birth" of a new *hpz*. Upon detection each *hpz* was assigned an ID number and it was tracked in time until it "died" (either due to pressure everywhere within the *hpz* dropping below the threshold pressure or due to a major failure event that resulted in a centroid shifting greater than half the *hpz* width). A typical example of a single *hpz* evolving in both space and time is shown in Fig. 3. On this basis, an empirical *hpz* is therefore defined as an extracted subset of tactile pressure sensor data, which consists of a single contiguous array of sensels having a pressure greater than or equal to the specified threshold pressure, and for which the "lifetime" of that empirical *hpz* is defined based on its criteria associated with its birth and death as defined earlier.

2.2 Methodology for Statistical *HPZ* Characterization. The development of a statistical description of *hpz*s requires extraction of detailed information about many individual *hpz*s. To develop these statistical distributions, the JOIA tactile pressure sensor data have been analyzed using the approach described in Sec. 2.1.2, and characteristics of each *hpz* have been extracted and used to populate a database. The database included characteristics of individual *hpz*s, such as areas, widths, heights, aspect ratios, perimeters, and *hpz* centroid positions (x, y), as well as pressure attributes including means, maximums, and standard deviations of *hpz* pressure. For each tactile sensor element inside the boundary of a given *hpz*, the elemental force was also calculated. Summing forces from all elements within an *hpz* boundary for a given instant yielded a record of *hpz* force as a function of time. Further, by multiplying this instantaneous force by the incremental indentation distance (i.e., the indentation speed multiplied by the time increment of the tactile sensor recording), an estimate of the energy dissipated through a given *hpz* could be obtained. Once all of the tactile sensor datasets had been processed using the automated *hpz* analysis routines, the empirical *hpz* data were then analyzed to extract information about high-pressure zone characteristics

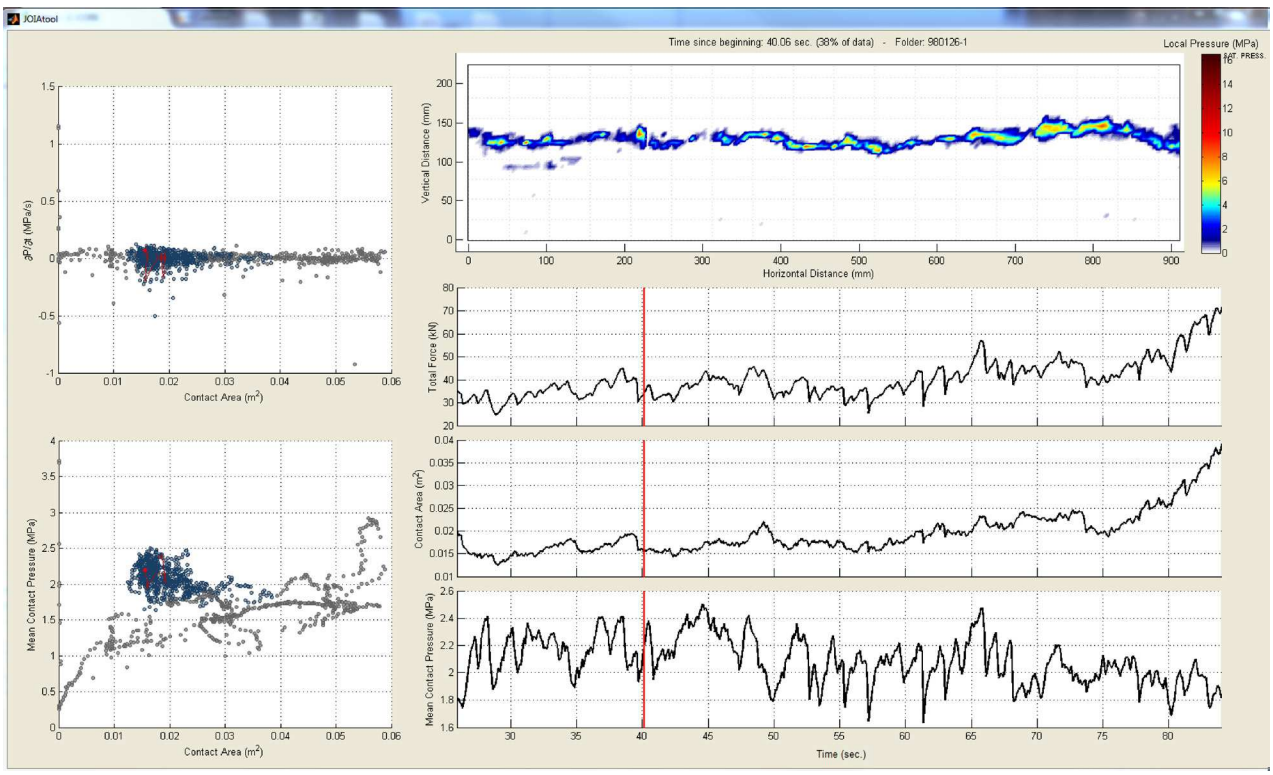

Fig. 2 Screenshot of the GUI of the JOIA analysis tool developed to assist in the analysis of the tactile sensor dataset

Downloaded From: https://offshoremechanics.asmedigitalcollection.asme.org on 05/03/2019 Terms of Use: http://www.asme.org/about-asme/terms-of-use

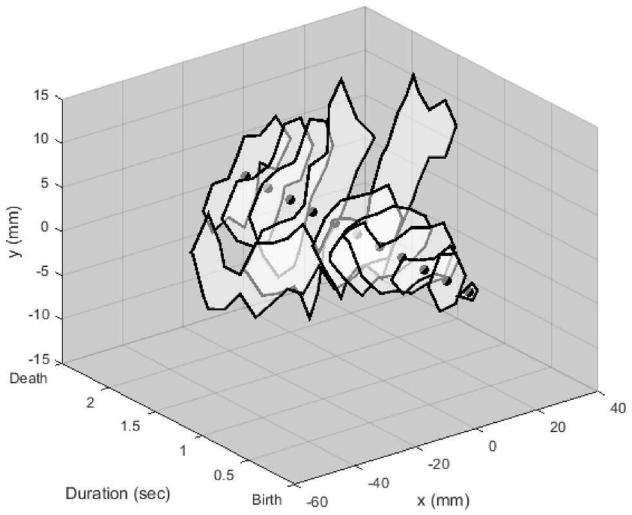

Fig. 3 Evolution of a single *hpz* in both space and time

such as distributions of *hpz* area, aspect ratio, location, duration, crushed depth, crushed volume, and pressure.

2.2.1 Effect of Pressure Threshold. The selection of a pressure threshold value to use in the identification and tracking of *hpz*s is an important consideration. To study how the characteristics of *hpz*s vary as a function of pressure threshold, these values have been varied in increments of 1 MPa, between values of 1 MPa and 10 MPa. The influence of pressure threshold on the percentage of total force carried and total energy dissipated by all *hpz*s is shown in Fig. 4. Similar results were obtained for both the slower indentation (0.3 cm/s) and faster indentation (3.0 cm/s) rates and the results do not appear to exhibit a strong dependence on indentation speed. At a given instant, the *hpz*s defined by a pressure threshold of 1 MPa will carry on average about 80% of the total load and dissipate about 80% of the energy during a given interaction.

The duration, crushed depth, and crushed volume of individual *hpz*s are also plotted as a function of lower pressure threshold for the two speeds considered. As seen from Fig. 5(*a*), the duration of individual *hpz*s is about an order of magnitude smaller for the higher indentation speeds. For a threshold value of 1 MPa, individual *hpz*s seem to survive for about 1 s at an indentation speed of 0.3 cm/s and about 0.1 s at an indentation speed of 3.0 cm/s. Correspondingly, the crushed depth of an *hpz* is taken as the total depth that the structure indents into the ice sheet before a given *hpz* is destroyed. This is calculated by multiplying the *hpz* duration by the indentation speed. The crushed depth for all *hpz*s in the database is shown in Fig. 5(*b*), where it can be seen that the mean *hpz* depth is roughly the same for both indentation speed for pressure thresholds values lower than 8 MPa. The mean depth of an *hpz*, based on this figure, would be around 3 mm, which corresponds to approximately 1% of the ice thickness (nominally 30 cm). It is worthwhile noting that the duration and depth of *hpz*s are relatively insensitive to threshold values below about 5 MPa, whereas the swept volume of individual *hpz*s is more sensitive, due to its dependence on contact area, which is more sensitive to threshold pressure Fig. 5(*c*). It is important to note that this choice of threshold pressure was a matter of judgment and not based on a physical rationale. While other values of threshold pressure may be used, it is essential any component of force associated with that threshold level which is excluded from the correspondingly defined *hpz*s be added back in through an appropriate background pressure factor *B*. For example, considering Fig. 4 we see that if a 1 MPa threshold captures regions that on average contain 80% of the force, then accurately modeling the total force necessitates inclusion of a factor to account for the remaining 20% of force

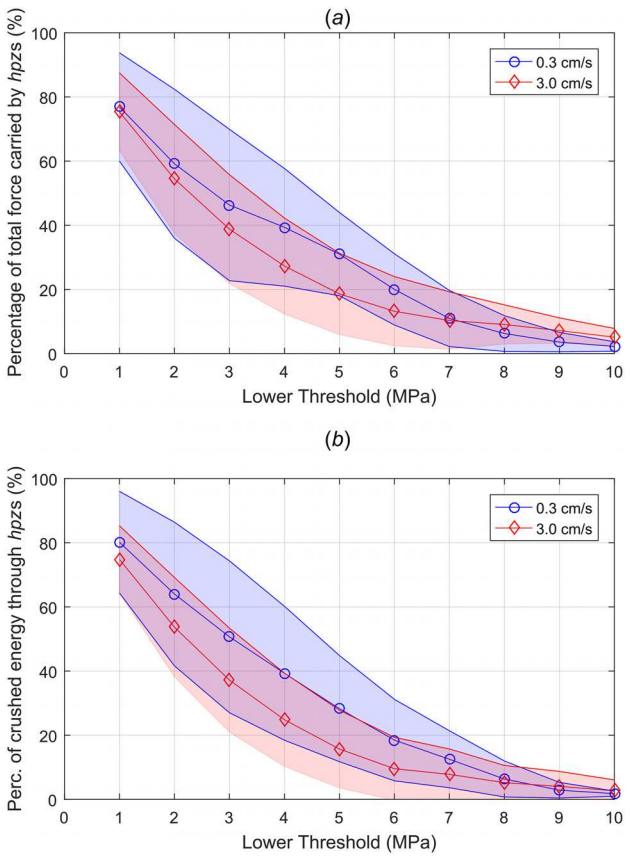

Fig. 4 Plots of (*a*) percentage of total force carried by all *hpz*s and (*b*) percentage of energy dissipated through *hpz*s as a function of lower pressure threshold for two interaction speeds. Shaded areas represent ±1 standard deviation around the mean.

outside the *hpz*s to avoid underestimating the total load. In this case, the background pressure factor would be calculated as $B = 0.20/0.80 = 0.25$. Similarly, considering Fig. 4, it is observed that if a pressure threshold of 2 MPa was used, this choice would result in an average of 60% of the total force being captured by the regions defined as *hpz*s, with the remaining 40% of force outside the *hpz*s that needing to be factored using a background pressure factor of $B = 0.40/0.60 = 0.67$. Based on the results discussed earlier, a constant value of threshold pressure of 1 MPa was selected for use throughout this analysis.

2.2.2 Area of High-Pressure Zones as Percentage of Total Area. To assess the percentage of the nominal interaction area that may be attributed to *hpz*s during an interaction, histograms of total contact areas as a percent of nominal interaction area for a pressure threshold value of 1 MPa have been plotted in Fig. 6. As may be observed, the percentage of nominal interaction area defined as *hpz*s spans a range from about 2% to 10% of the nominal interaction area, with a mean of about 5% of total area for both speed ranges.

From prior analyses of the JOIA tactile sensor data [24,25], it has been observed that the total contact area during an interaction when no threshold pressure is used is on the order of about 10% of the nominal interaction area. Since a portion of the total contact area will correspond to a lower background pressure that is below the 1 MPa threshold value used to define individual *hpz*s in this analysis, the total *hpz* area (e.g., sum of all *hpz* areas above the pressure threshold) will include only a subset (about 50% on average) of the sensor elements contained in the total contact area.

2.2.3 Area of Individual High-Pressure Zones. Since there are many individual *hpz*s present at any given instant, the total *hpz*

Downloaded From: https://offshoremechanics.asmedigitalcollection.asme.org on 05/03/2019 Terms of Use: http://www.asme.org/about-asme/terms-of-use

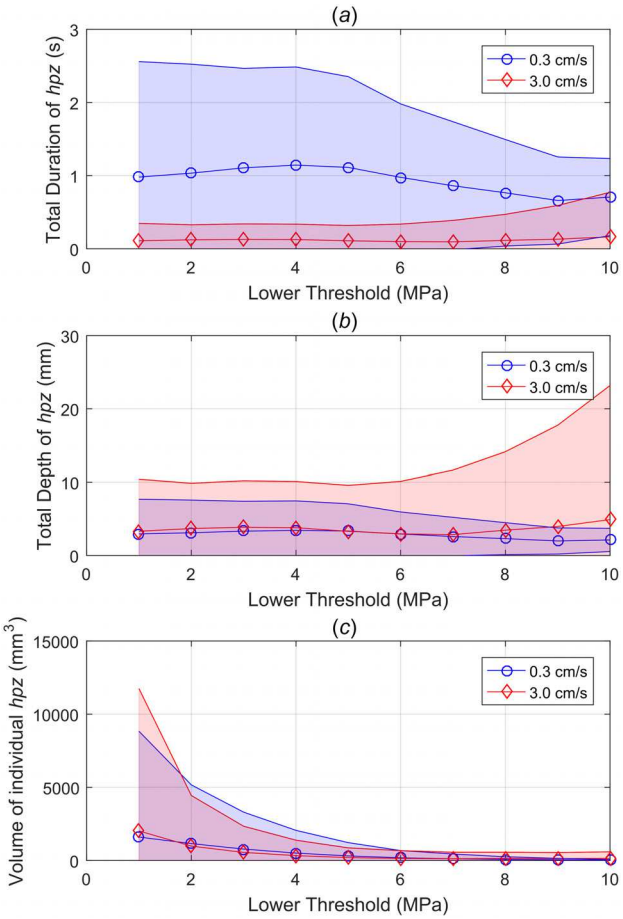

Fig. 5 Plots of (*a*) duration, (*b*) total crushed depth, and (*c*) total crushed volume of individual *hpz*s as a function of lower pressure threshold. Shaded areas represent ±1 standard deviation around the mean.

areas represented in Fig. 6 will be comprised of many individual *hpz* areas. As shown from the histograms given in Fig. 7, for the conditions present during the JOIA test program, individual *hpz* areas may be up to a few thousand square millimeters in size, though the majority of these *hpz*s will on the order of less than a hundred square millimeters. Considering the data for an individual *hpz* given in Fig. 3, it should be noted that the contact area for a given *hpz* may evolve considerably over the lifetime of the *hpz*.

2.2.4 Crushed Depth and Crushed Volume. As noted earlier, crushed depth is calculated by multiplying the duration of *hpz*s with the indentation speed. Figure 8 shows histogram of crushed depth in the direction of indentation for the two different speeds used in the JOIA test program. It is noted that here an offset value has been used to discard the depths which are very close to zero (<0.5 mm). The similarity in the trend shown in the histogram suggests that for the given range of speeds, *hpz* failure depth is collectively consistent irrespective of the indentation speed. Such observations have important implications since these results suggest that the load transmitting mechanism may be dominated by characteristic failure processes in the ice rather than indentation speed alone.

For each time-step during the lifetime of an *hpz*, an incremental crushed volume value may be estimated by multiplying the instantaneous *hpz* area on the vertical plane by the incremental crushed depth for that time-step. Summing all incremental crushed volumes over the duration of the *hpz* yields the total crushed volume for each individual *hpz*. For the entire population of *hpz*s in the database, the crushed volume values have been calculated and histograms corresponding to each speed are given in Fig. 9. From

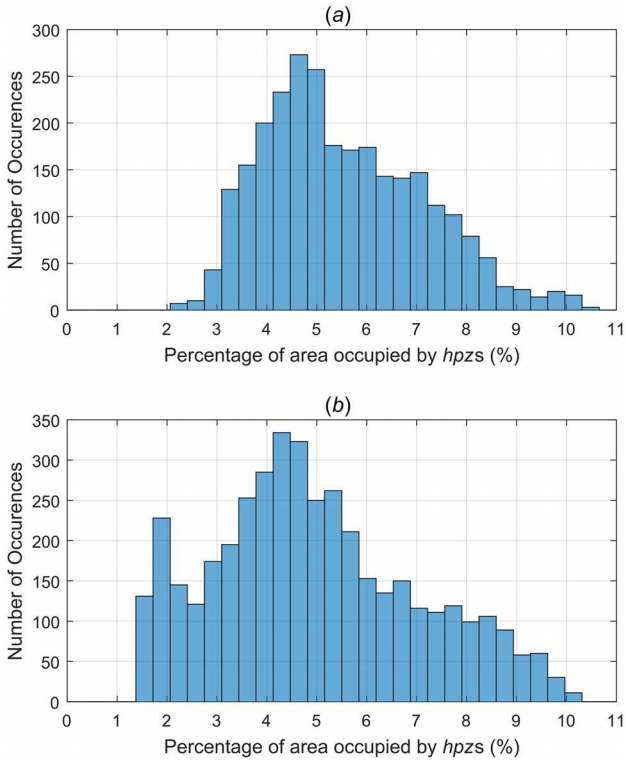

Fig. 6 Histogram of total *hpz* area as a percentage of nominal interaction area for each frame, for indentation speed of (*a*) 0.3 cm/s and (*b*) 3.0 cm/s

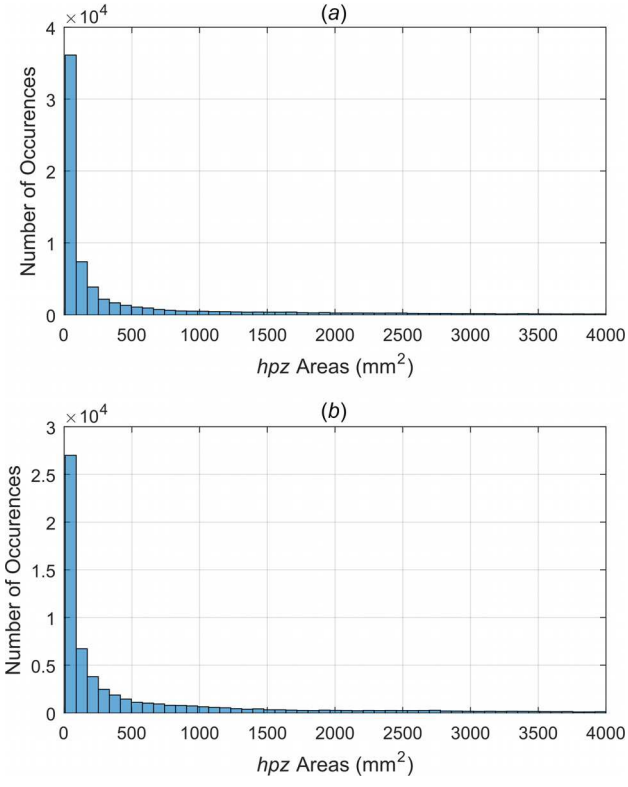

Fig. 7 Histogram of the *hpz* area (includes all time steps within an *hpz* "life") for indentation speed of (*a*) 0.3 cm/s and (*b*) 3.0 cm/s

Downloaded From: https://offshoremechanics.asmedigitalcollection.asme.org on 05/03/2019 Terms of Use: http://www.asme.org/about-asme/terms-of-use

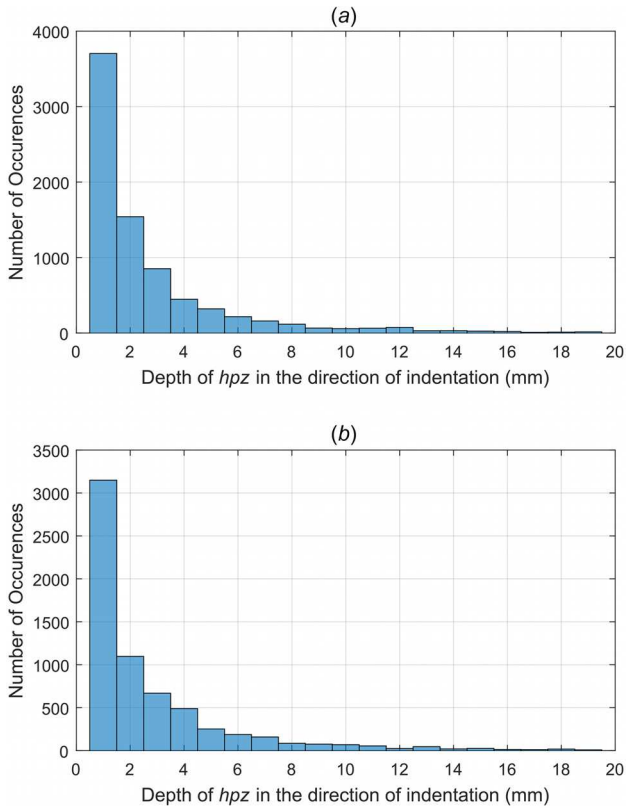

Fig. 8 Histogram of crushed depth for individual *hpz*s for indentation speed of (*a*) 0.3 cm/s and (*b*) 3.0 cm/s

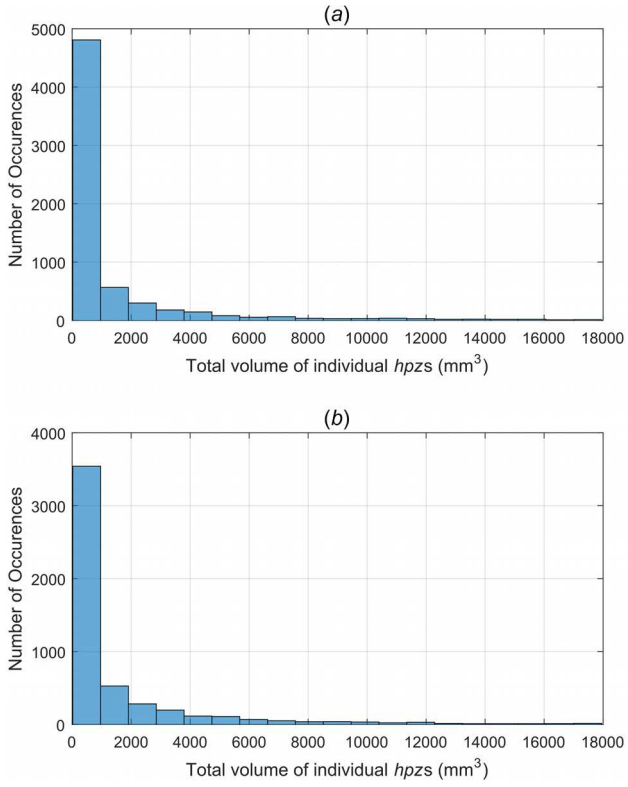

Fig. 9 Histogram of the crushed volume of individual *hpz* for indentation speed of (*a*) 0.3 cm/s and (*b*) 3.0 cm/s

this figure, it is seen that the distribution of crushed ice volumes is approximately the same for both indentation speeds.

Two critically important pieces of information may be observed from Figs. 8 and 9 for the indentation speeds and ice conditions considered:

(i) The distribution of the crushed depth is relatively insensitive to indentation rate, and
(ii) The distribution of the crushed volume is relatively insensitive to indentation rate.

While it is well understood that, in general, time dependence is highly important in ice failure behavior processes (these effects may be more pronounced for different temperatures or salinities), the above data suggest that it is reasonable to treat the crushed layer depth and volume distributions as being relative constant for the range of speeds considered.

2.2.5 Peak Pressures and Force Within Individual Hpzs. To assess the distribution of peak pressure and force within individual *hpz*s, the empirical cumulative distribution functions (CDFs) for both speed ranges were plotted in Figs. 10 and 11, respectively. From Fig. 10, it may be observed that the mean value of the peak *hpz* pressure is approximately 3 MPa for both speed ranges. This pressure intensity is considerably lower than reported for confined multiyear ice [20,28] and further work is recommended to improve the understanding of how *hpz* pressure and force intensities scale for different ice loading scenarios and temperatures.

2.2.6 Spatial and Temporal Distribution of Hpzs. To assess the spatial and temporal behavior of individual *hpz*s, the mean trajectory (path traced in space–time by the centroid of each *hpz* over its lifetime) has been plotted in Fig. 12. In this plot, the length of each individual line represents the depth of a single *hpz*. Correspondingly, the depth of each *hpz* may be determined from the length of each line, which is calculated as the difference between the maximum and minimum indentation depths for that individual *hpz*. This result shows that the size of individual, independent *hpz*s is significantly smaller and the spatial density of *hpz*s is much higher when compared with values estimated from pressure panel data [11,16].

2.3 Methodology for Design Load Estimation. Individual *hpz*s exhibit significant spatial and temporal variability during their lifetime. For multiple *hpz*s acting over a region, the nonsimultaneous nature of the loads transmitted by these *hpz*s results in the averaging of loads over the total interaction area. As a consequence of this pressure averaging phenomenon, global pressures

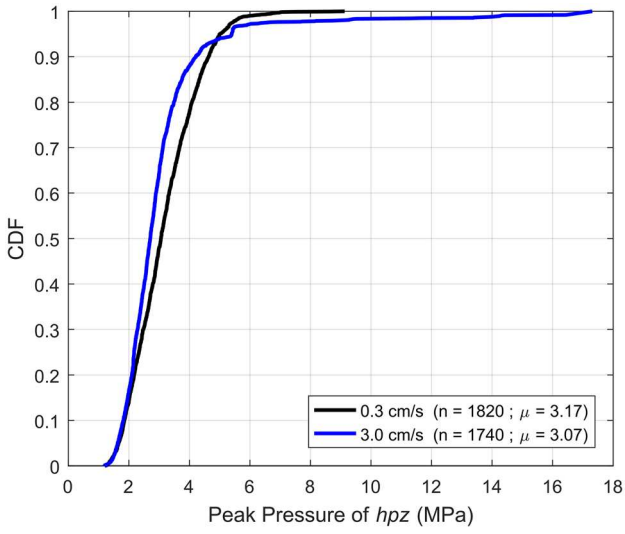

Fig. 10 Peak pressure CDFs within *hpz*s for indentation speed of 0.3 cm/s and 3.0 cm/s

Downloaded From: https://offshoremechanics.asmedigitalcollection.asme.org on 05/03/2019 Terms of Use: http://www.asme.org/about-asme/terms-of-use

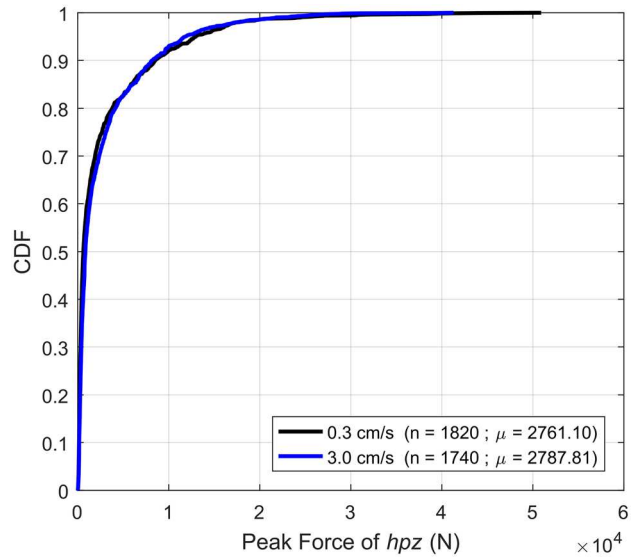

Fig. 11 CDF of peak force within *hpz*s for indentation speed of 0.3 cm/s and 3.0 cm/s

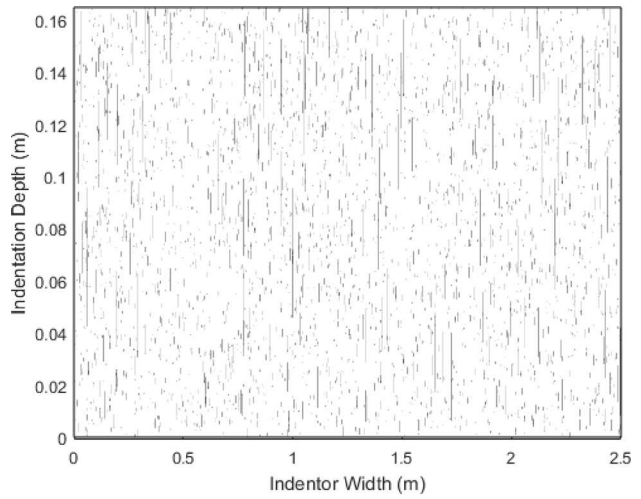

Fig. 12 Plot of mean indentation trajectories of individual *hpz*s showing both spatial distribution (represented by horizontal location) and indentation depth, which also indicates the duration of each *hpz* (represented by length of the line)

have a reduced variance when compared with local pressures. To capture the effects of variance reduction when extrapolating local pressures to the case of global areas, various pressure averaging models have been developed [12,14,38–40]. Such models provide important insights into variance reduction effects for global pressures as a function of increased width but do not fully account for local pressure scale effects. To address these gaps, details of *hpz* behavior and associated load limiting mechanisms need to be considered.

For the purpose of the present model, the concentration of *hpz*s into such patterns is handled through the introduction of a geometrically linked "contact area envelope" (CAE). The CAE is defined as an idealized geometric region of the ice contact interface in which all *hpz*s will occur and through which *hpz* loads are transmitted. As illustrated in Fig. 13, the CAE is modeled here as a function of the global area based on the geometric model of Spencer and Masterson [26] for both low aspect ratio (top) and high aspect ratio (bottom) cases. As discussed by Jordaan et al. [3], for the purposes of design the global interaction area is defined as the total projected area of the ice feature onto the structure, while the local design area corresponds to some fixed region on the structure such as a plate between frames. The areas of individual *hpz*s are defined as the evolving regions of localized ice–structure contact through which the majority of loads are transmitted to the structure. Each empirical *hpz* that is sampled from the database [36] has an associated area–time series (e.g., a variant of the area–time data shown in Fig. 3), which defines how the area of that *hpz* will vary in time. The relationships between these different areas definitions are shown in Fig. 13.

In general, the occurrence of *hpz*s within the CAE may be considered as a birth and death process. Since in the present model the evolution and death of each *hpz* are embodied in the time-series data for each sampled empirical *hpz*, only the birth rate needs to be modeled as a Poisson arrival process. In implementing this model, the arrival locations and times may be mapped out using an average spatial–temporal *hpz* density ψ_{hpz} which can be used to map randomly drawn *hpz*s to locations across the centerlines of the CAE in time. The purpose of the CAE in the model is to define the region of the ice in which the sampled *hpz*s are mapped, which in turn influences how associated modeled loads are concentrated on the structure. Since this is an empirical approach, it is important to recognize that the pressures associated with these empirical *hpz*s are necessarily linked to the ice conditions corresponding to the JOIA data. As is discussed in ISO 19906, differences may be expected between the index strength (e.g., uniaxial compressive strength) of ice in a region of interest for design and the index strength of the ice from the region corresponding to the data used to develop an empirical methodology. In ISO 19906, Eq. A.8-22 suggests that an index strength factor $\lambda = \frac{\sigma}{\sigma_0}$ may be used where σ is the index strength for the area of interest for design, and σ_0 is the index strength for the reference dataset used to derive the empirical relationship.

For a given interaction, the total load F_T acting over the area of interest may be calculated as the sum of loads $F_{\mathrm{HPZ},i}$ transmitted through each of the ith *hpz*s acting on that region, as well as a component of force associated with background ice pressure. As described by Richard and Taylor [36], results from an analysis of JOIA tactile sensor data suggest that this background pressure component may be modeled being some proportion of the *hpz* load. It is important to note that the physical basis for this background pressure lies in the presence of fragmented and crushed ice at the ice–structure interface, which surround these high-pressure zones and through which a lower, but non-negligible level of pressure is applied to the structure. Accounting for the index strength factor λ and introducing such a background pressure factor B, the total load acting over a region can be written using the following simplified expression [41,42]:

$$F_T = \lambda \sum (F_{\mathrm{HPZ},i})(1 + B) \tag{1}$$

It is important to recall that the pressure threshold value used in the analysis of individual *hpz*s plays an important role in determining the amount of total load attributed to the individual *hpz*s and the proportion attributed to background pressures. It is therefore essential that the magnitude of the factor B appropriately accounts for the proportion of load carried by all *hpz*s, which in turn is a function of the selected threshold value used in the extraction of the *hpz* data.

3 Illustrative Example: Design Load Estimation

Using the methodology described in Sec. 2.3 along with the empirical descriptions of *hpz* attributes presented earlier, a series of force–time simulations have been conducted. For all cases, the structure is modeled as a vertical-faced structure interacting with a level ice sheet having a thickness of $h = 0.27$ m (average ice thickness of the tests considered from JOIA data). Three different structure widths were considered for the analysis with a background pressure factor of 0.25. Based on the JOIA data, the

Downloaded From: https://offshoremechanics.asmedigitalcollection.asme.org on 05/03/2019 Terms of Use: http://www.asme.org/about-asme/terms-of-use

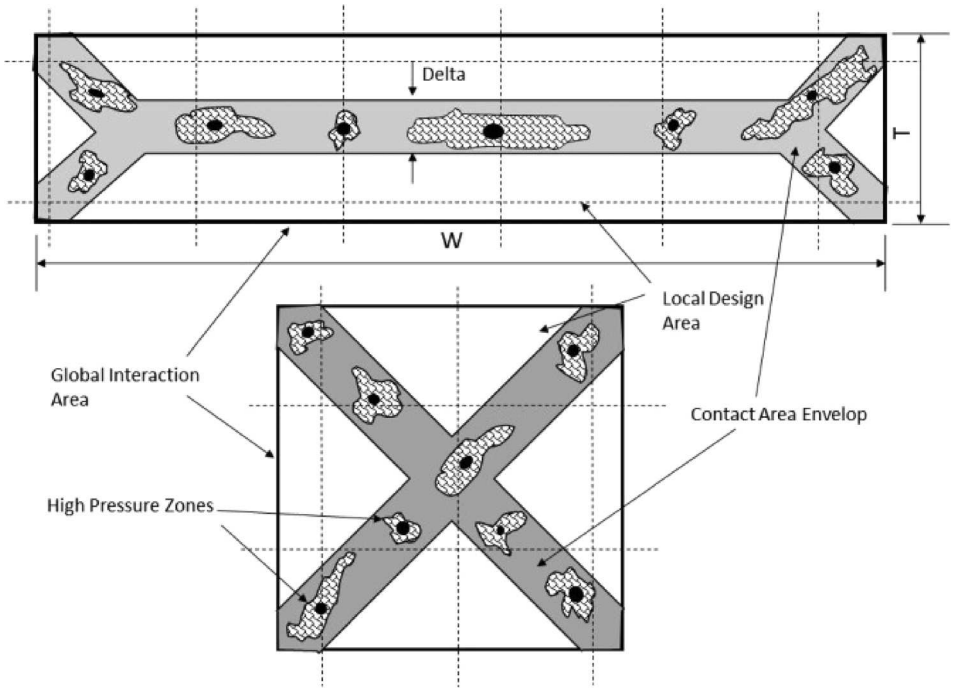

Fig. 13 Illustrations of idealized relationships between global interaction area, local design area (dashed line represents stiffeners between plates), CAE (gray-shaded region), and *hpz*s (hatched areas) for low aspect ratio (top) and high aspect ratio (bottom)

spatial–temporal *hpz* density ψ_{hpz} may be estimated to be $23\,\mathrm{m}^{-1}\mathrm{s}^{-1}$ for a pressure threshold of 1 MPa and birth event of *hpz*s may be simulated as a random Poisson arrival process both spatially and temporally. As may be observed from Fig. 14, the mean value of force-per-unit width for all the three simulated datasets corresponds well with the dashed line representing the mean value from the measured data. The parallel lines to the mean dashed line represent bounds for one standard deviation, and by comparison, the simulated data indicate that the standard deviation of the force-per-unit width decreases as a function of increasing width. These observations of a constant mean pressure and a decreasing variance for increasing width are consistent with random averaging theory (e.g., see Ref. [43]). From a physical viewpoint, this is consistent as well since the loads acting over a narrow region would be dominated by either a single *hpz* or a small number of *hpz*s, while loads over a wide region would be transmitted through many *hpz*s. As a consequence, for narrow regions, the occurrence of random local processes, such as spall events near a given *hpz*, would proportionally have much more of an impact on the total load than it would on the total load acting over a wide region. As may be seen in Fig. 14 for the case of the region having a width of 0.15 m, there are periods of very high force-per-unit width as well as regions of low or no load (due to local ice failure events which can result in gaps in contact). For the case of the 1.5 m and 15 m regions, failure of individual *hpz*s would not result in a load drops completely to zero, since loads will continue to be transmitted through other *hpz*s acting on the structure.

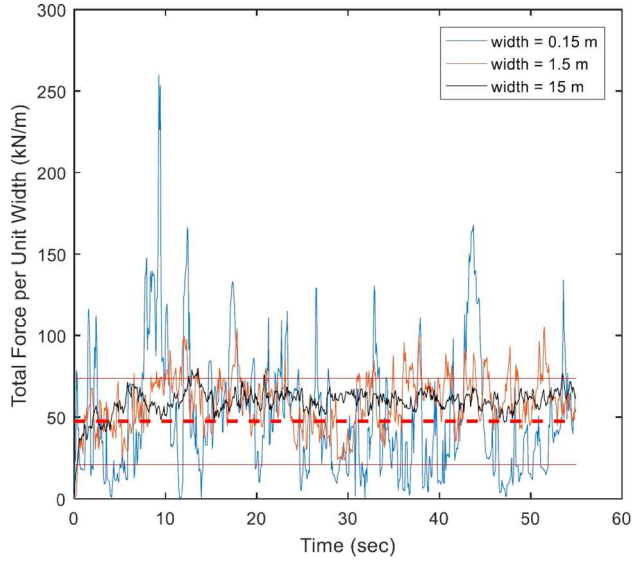

Fig. 14 Plot of simulated time series data for force-per-unit width for three structure widths (0.15 m, 1.5 m, and 15 m) compared with the event mean pressure (dashed line)

To compare results from the *hpz*-based model with those obtained using established local and global pressure models, the case of a thin, first-year ice sheet ($h = 0.3$ m) interacting with a vertical-walled structure has been simulated, see Fig. 5. The global pressure model used for comparison is based on ISO 19906 [1] Eq. A.8-21 with an ice strength coefficient of $C_R = 1.8$ (based on Baltic Sea ice data).

The local pressure design method for first-year sea ice given in Section A.8.2.5.2 of the ISO 19906 code is unclear and implies that pressure is dependent only on thickness and not on width, which does not reflect observations from full-scale measurements. To provide a more representative basis for comparison, the event-maximum methodology from Section A.8.2.5.4 was used [1]. In this model, the extreme load z_e is calculated using the expression:

$$z_e = x_0 + \alpha\left\{-\ln\left[-\ln F_z(z_e)\right] + \ln v + \ln r\right\} \tag{2}$$

where x_0 is a constant and α is an area-dependent relationship determined from representative ship–ice impact data (see Refs. [8] and [13] for additional detail of how these parameter values are determined). $F_z(z_e)$ is the exceedance probability, v is the expected number of events, and r is the expected proportion of hits. The local pressure curve presented in Fig. 15 corresponds with values of $F_z(z_e) = 0.99$ (e.g., 100-year load), $v = 5 \times 10^3$,

Downloaded From: https://offshoremechanics.asmedigitalcollection.asme.org on 05/03/2019 Terms of Use: http://www.asme.org/about-asme/terms-of-use

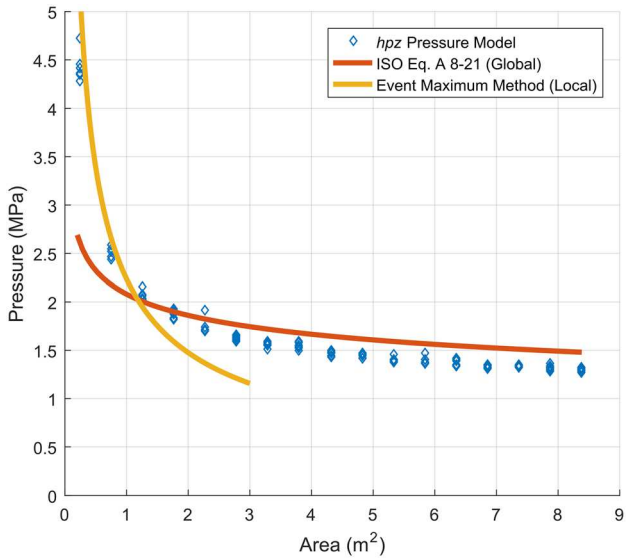

Fig. 15 Comparison of simulated pressure–area data from *hpz* model, ISO global pressure model, and event-maximum method

$r = 0.5$, and $x_0 = 0$. The parameter α is modeled using the expression $\alpha = CA^D$, where A is the area of interest, and values of coefficient $C = 0.18$ and exponent $D = -0.6$ are empirical constants determined from the analysis of ice impact data from the Canadian Coast Guard Ship Louis S. St. Laurent in ice conditions representative of those of interest in the present analysis [13].

The data for the *hpz* pressure model given in Fig. 15 were calculated by simulating the total force transmitted through individual *hpz*s which have been mapped to the CAE and simulated for defined increments of global contact area and interaction duration. For the purposes of comparison, peak pressures are taken as the values corresponding to the mean plus three standard deviations of pressure for a given area. Since the individual *hpz*s within a simulated event will be randomly sampled from the database, variation in peak pressure estimates will result for each simulation run. To illustrate the spread of the simulated results, multiple repetitions were generated for each area increment, as is shown in Fig. 15. To account for the differences between the index (uniaxial compressive) strength for the ice tested in the JOIA program (e.g., see Ref. [33]) and the index to "Baltic Sea" ice (e.g., see Ref. [44]) corresponding the ISO design curves, an index strength factor of $\frac{\sigma}{\sigma_0} \approx 2.5$ was used. This approach is similar to the approach used in Eq. A.8-22 in ISO 19906 to account for difference between index strengths between a given region of interest and that of the reference region.

For the case of thin first-year sea ice, the analysis simplifies since it is reasonable to assume that the local design area is fully enveloped by the thickness of the ice. Therefore, in this special case, the local area is defined by the ice thickness and the width of the panel area of interest. In its limit the maximum design area width equals the structure width (e.g., is the same as global area). Since the global interaction area is a function of ice thickness and structure width, for the special case of thin first-year sea ice, the local pressure–area curve and the global pressure–area use consistent area definitions, yielding the same pressure curve (assuming the same exposure level). If one is interested in the maximum local pressure on all panels of width w_L on a structure of total width w_G, then the exposure rate for that local area A_L must be increased by $\chi = \frac{w_L}{w_G}$ to account for the number χ of local areas of size A_L within the global interaction area A_G. Examining the results shown in Fig. 15, it may be concluded that the *hpz* pressure model provides results which have good general agreement with estimates obtained from established local and global pressure metholodolgy. Further research is planned to continue development of this methodology as a means to model local and global pressures and to extend this model to other ice conditions and interaction scenarios.

4 Discussion and Conclusion

High-resolution tactile pressure sensor data provide significant additional insight into the nature of interface pressure behavior during ice–structure interactions than can be inferred from load panel measurements alone. The present analysis indicates that for the ice conditions during the JOIA test program, the contact interface is expected to be loaded through many small independently varying *hpz*s rather than through a few large *hpz*s, as might be inferred if loads were measured by a single panel. However, the percentage of total area covered by these *hpz*s at a particular instant is still very small compared to the global interaction area. The spatial and temporal variation of these independent *hpz*s have important implications for the development of theoretical models since it is important to understand if correlations arise from failure processes in the ice or if apparent correlations are a consequence of pressure averaging over the measurement area. Statistical characterization of different *hpz* properties was shown to provide important insights into the different attributes of the features, which offer potential directions for linking underpinning physics with the ensemble behavior of *hpz*s and the global failure behavior of ice. For the range of speeds from the JOIA data considered here, it was found that *hpz* depths are consistent irrespective of indentation speed. Such observation suggests that the *hpz* failure behavior is dominated by ice failure processes, rather than simply being a function of the interaction speed. Another important feature of these data is that the distribution of maximum indentation depth associated with the failure of each *hpz* indicates that there may be a consistent, characteristic failure depth distribution associated with high-pressure zones at this scale. This observation is consistent with prior assessments based on a combination of damage layer theory (e.g., see Ref. [21]) and probabilistic modeling of fracture (e.g., see Refs. [13] and [45]). Links between the characteristic distributions presented here and underpinning mechanics are the subject of ongoing research.

The model presented here, which is based on extracted characteristics of *hpz*s from JOIA tactile pressure sensor data, yields promising results for helping understand the nature of pressure–area curves used for design ice load estimation. This approach serves to provide a framework for linking ongoing research on fundamental aspects of individual *hpz* behavior with design methodology based on ensemble behavior of all *hpz*s acting over a given region. As with any model based on empirical results, one must carefully consider how well the conditions associated with the data used in developing the model reflect the conditions to which the model is being applied. For the present work, emphasis has been placed on thin first-year sea ice at warm temperatures. Factors such as ice thickness, temperature, ice type, and other physical conditions may influence the resulting *hpz* pressures and these factors need to be considered further. For interactions involving multiyear sea ice, local pressures much higher than those observed in the JOIA program have been reported (e.g., see Refs. [20], [27], and [28]). Further work is needed to extend the present work beyond the case of thin first-year sea ice and additional field-scale tactile sensor data are needed to help advance understanding of *hpz* attributes, their ensemble behavior, and associated scaling issues.

Through the development of new models that reflect the behavior of *hpz*s and which can be more clearly linked to the mechanics of compressive ice failure, greater confidence in design ice load estimation can be realized.

Acknowledgment

Financial support from the Research Development Corporation of Newfoundland and Labrador (RDC) is gratefully acknowledged. The authors would like to acknowledge the Japan Ocean Industries Association (JOIA) for making these data available and

Downloaded From: https://offshoremechanics.asmedigitalcollection.asme.org on 05/03/2019 Terms of Use: http://www.asme.org/about-asme/terms-of-use

also Dr. Robert Frederking of the National Research Council of Canada and Dr. Ian Jordaan of Memorial University for their help during the initial processing and analysis of these data. Financial support from the Research Development Corporation of Newfoundland and Labrador (RDC) is gratefully acknowledged.

Funding Data

- Natural Sciences and Engineering Research Council of Canada (Funder ID. 10.13039/501100000038).
- Research Development Corporation of Newfoundland and Labrador (RDC).

References

[1] ISO, 2010, "Petroleum and Natural Gas Industries—Arctic Offshore Structures," International Organization for Standardization, Geneva, Switzerland, Standard No. 19906.

[2] Sanderson, T. J. O., 1988, *Ice Mechanics: Risks to Offshore Structures*, Graham & Trotman, Boston, MA.

[3] Jordaan, I., Li, C., and Sudom, D., 2005, "Principles for Local and Global Ice Design Using Pressure-Area Relationships," 18th International Conference on Port and Ocean Engineering Under Arctic Conditions, New York, June 26–30, pp. 375–385.

[4] Masterson, D., Frederking, R., and Wright, B., 2007, "A Revised Ice Pressure-Area Curve," 19th International Conference on Port and Ocean Engineering Under Arctic Conditions, Dalian, China, June 27–30, pp. 305–314.

[5] Palmer, A. C., Dempsey, J. P., and Masterson, D. M., 2009, "A Revised Ice Pressure-Area Curve and a Fracture Mechanics Explanation," Cold Reg. Sci. Technol., **56**(2–3), pp. 73–76.

[6] Timco, G. W., and Sudom, D., 2013, "Revisiting the Sanderson Pressure–Area Curve: Defining Parameters That Influence Ice Pressure," Cold Reg. Sci. Technol., **95**(Suppl. C), pp. 53–66.

[7] Maes, M. A., 1992, "Probabilistic Behaviour of a Poisson Field of Flaws in Ice Subjected to Indentation," 11th IAHR International Symposium on Ice, Banff, AB, Vol. 2, pp. 871–882.

[8] Jordaan, I. J., Maes, M. A., and Brown, P. W., 1993, "Probabilistic Analysis of Local Ice Pressures," ASME J. Offshore Mech. Arct. Eng., **115**(1), pp. 83–89.

[9] Kujula, P., 1994, "On the Statistics of Ice Loads on Ship Hull in the Baltic," Ph.D. thesis, Helsinki University of Technology, Espoo, Finland.

[10] Zou, B., 1996, "Ships in Ice: The Interaction Process and Principles of Design," Ph.D. thesis, Memorial University of Newfoundland, St. John's, NL.

[11] Johnston, M. E., Croasdale, K. R., and Jordaan, I. J., 1998, "Localized Pressures During Ice–Structure Interaction: Relevance to Design Criteria," Cold Reg. Sci. Technol., **27**(2), pp. 105–117.

[12] Jordaan, I., Frederking, R., and Li, C., 2006, "Mechanics of Ice Compressive Failure, Probabilistic Averaging and Design Load Estimation," 18th IAHR International Symposium on Ice, Sapporo, Japan, Aug. 28–Sept. 1, pp. 223–230.

[13] Taylor, R. S., Jordaan, I. J., and Li, C., 2010, "Local Design Pressures for Structures in Ice: Analysis of Full-Scale Data," ASME J. Offshore Mech. Arct. Eng., **132**(3), p. 031502.

[14] Spencer, P. A., and Morrison, T. B., 2012, "High Pressure Zones, Statistics and Pressure-Area Effects," International Conference and Exhibition on Performance of Ships and Structures in Ice 2012, Banff, AB, Sept. 17–20, pp. 179–184.

[15] Kujala, P., and Arughadhoss, S., 2012, "Statistical Analysis of Ice Crushing Pressures on a Ship's Hull During Hull–Ice Interaction," Cold Reg. Sci. Technol., **70**(1), pp. 1–11.

[16] Spencer, P., 2013, "Unifying Local and Global Ice Crushing Pressures," 22nd International Conference on Port and Ocean Engineering Under Arctic Conditions, Espoo, Finland.

[17] Suyuthi, A., Leira, B. J., and Riska, K., 2014, "A Generalized Probabilistic Model of Ice Load Peaks on Ship Hulls in Broken-Ice Fields," Cold Reg. Sci. Technol., **97**(1), pp. 7–20.

[18] Ralph, F., and Jordaan, I., 2017, "Local Design Pressures During Ship Ram Events Modeling the Occurrence and Intensity of High Pressure Zones," ASME Paper No. OMAE2017-62545.

[19] Kotilainen, M., Vanhatalo, J., and Suominen, M., 2017, "Predicting Ice-Induced Load Amplitudes on Ship Bow Conditional on Ice Thickness and Ship Speed in the Baltic Sea," Cold Reg. Sci. Technol., **135**(1), pp. 116–126.

[20] Frederking, R., Jordaan, I., and McCallum, J., 1990, "Field Tests of Ice Indentation at Medium Scale: Hobson's Choice Ice Island 1989," Tenth IAHR International Symposium on Ice, Espoo, Finland, Vol. 2, pp. 931–944.

[21] Jordaan, I. J., 2001, "Mechanics of Ice-Structure Interaction," Eng. Fract. Mech., **68**(17–18), pp. 1923–1960.

[22] Riska, K., 1991, "Observations of the Line-Like Nature of Ship-Ice Contact," 11th International Conference on Port and Ocean Engineering Under Arctic Conditions, St. John's, NL, Vol. 2, pp. 785–811.

[23] Sodhi, D. S., Takeuchi, T., and Kawamura, M., 2001, "Measurement of Ice Forces and Interfacial Pressure During Medium-Scale Indentation Tests in Japan," 16th International Conference on Port and Ocean Engineering Under Arctic Conditions, Ottawa, ON, Canada, Aug. 12–17, pp. 617–626.

[24] Frederking, R., 2004, "Ice Pressure Variations During Indentation," 17th IAHR International Symposium on Ice, Saint Petersburg, Russia, June 21–25, pp. 307–314.

[25] Taylor, R. S., Frederking, R. F., and Jordaan, I. J., 2008, "The Nature of High Pressure Zones in Compressive Ice Failure," 19th IAHR International Symposium on Ice, Vancouver, BC, June 6–11, pp. 1001–1010.

[26] Spencer, P. A., and Masterson, D., 1993, "Geometrical Model for Pressure Aspect-Ratio Effects in Ice-Structure Interaction," ASME Paper No. 93-215.

[27] Glen, I., and Blount, H., 1984, "Measurement of Ice Impact Pressures and Loads Onboard CCGS Louis S. St. Laurent," Third International Offshore Mechanics and Arctic Engineering Symposium, New Orleans, LA, Feb. 12–17.

[28] Masterson, D. M., and Frederking, R. M. W., 1993, "Local Contact Pressures in Ship/Ice and Structure/Ice Interactions," Cold Reg. Sci. Technol., **21**(2), pp. 169–185.

[29] Mackey, T., Wells, J., and Jordaan, I., 2007, "Experiments on the Fracture of Polycrystalline Ice," 19th International Conference on Port and Ocean Engineering Under Arctic Conditions, Dalian, China, Vol. 1, pp. 339–349.

[30] Wells, J., Jordaan, I., and Derradji-Aouat, A., 2011, "Small-Scale Laboratory Experiments on the Indentation Failure of Polycrystalline Ice in Compression: Main Results and Pressure Distribution," Cold Reg. Sci. Technol., **65**(3), pp. 314–325.

[31] Takeuchi, T., Masaki, T., and Akagawa, S., 1997, "Medium-Scale Field Indentation Tests (MSFIT)—Ice Failure Characteristics in Ice/Structure Interactions," Seventh International Offshore and Polar Engineering Conference, Honolulu, HI, May 25–30, Paper No. ISOPE-I-97-209.

[32] Matsushita, H., Takawaki, T., and Masaki, K., 1997, "Medium Scale Field Indentation Tests-Physical Properties and Strength of the Ice Sheet," Seventh International Offshore and Polar Engineering Conference, Honolulu, HI, May 25–30, Paper No. ISOPE-I-97-208.

[33] Kamio, Z., Takawaki, T., and Matsushita, H., 2000, "Medium Scale Field Indentation Tests: Physical Characteristics of First-Year Sea Ice at Notoro Lagoon, Hokkaido," Tenth International Offshore and Polar Engineering Conference, Seattle, WA, May 28–June 2, Paper No. ISOPE-I-00-082.

[34] Matsushita, H., Kamio, Z., and Sakai, M., 2000, "Consideration of Failure Mode of a Sea Ice Sheet," Tenth International Offshore and Polar Engineering Conference, Seattle, WA, May 28–June 2, Paper No. ISOPE-I-00-084.

[35] Takeuchi, T., Akagawa, S., and Kawamura, M., 2000, "Examination of Factors Affecting Total Ice Load Using Medium Scale Field Indentation Test Data," Tenth International Offshore and Polar Engineering Conference, Seattle, WA, May 28–June 2, Paper No. ISOPE-I-00-089.

[36] Richard, M., and Taylor, R. S., 2014, "Analysis of High Pressure Zone Attributes from Tactile Pressure Sensor Field Data," ASME Paper No. OMAE2014-24342.

[37] Akagawa, S., Nakazawa, N., and Sakai, M., 2000, "Ice Failure Mode Predominantly Producing Peak-Ice-Load Observed in Continuous Ice Load Records," Tenth International Offshore and Polar Engineering Conference, Seattle, WA, May 28–June 2, Paper No. ISOPE-I-00-089.

[38] Dunwoody, A., 1991, "Non-Simultaneous Ice Failure," Amoco Production, Tulsa, OK, Report.

[39] Sodhi, D. S., Takeuchi, T., and Nakazawa, N., 1998, "Medium-Scale Indentation Tests on Sea Ice at Various Speeds," Cold Reg. Sci. Technol., **28**(3), pp. 161–182.

[40] Taylor, R. S., and Jordaan, I. J., 2011, "The Effects of Non-Simultaneous Failure, Pressure Correlation, and Probabilistic Averaging on Global Ice Load Estimates," 21st International Offshore and Polar Engineering Conference, Maui, HI, June 19–24, Paper No. ISOPE-I-11-340.

[41] Taylor, R. S., and Richard, M., 2014, "Methodology for Combined Local and Global Ice Pressure Estimation Based on a Probabilistic Model of High Pressure Zone Behavior Derived from Field Data," Arctic Technology Conference, Houston, TX, Feb. 10–12, Paper No. OTC-24631-MS.

[42] Taylor, R. S., and Richard, M., 2014, "Development of a Probabilistic Ice Load Model Based on Empirical Descriptions of High Pressure Zone Attributes," ASME Paper No. OMAE2014-24353.

[43] Vanmarcke, E., 2010, *Random Fields: Analysis and Synthesis*, World Scientific, Singapore.

[44] Jones, S. J., 1997, "High Strain-Rate Compression Tests on Ice," J. Phys. Chem. B, **101**(32), pp. 6099–6101.

[45] Taylor, R. S., and Jordaan, I. J., 2015, "Probabilistic Fracture Mechanics Analysis of Spalling During Edge Indentation in Ice," Eng. Fract. Mech., **134**(1), pp. 242–266.

Downloaded From: https://offshoremechanics.asmedigitalcollection.asme.org on 05/03/2019 Terms of Use: http://www.asme.org/about-asme/terms-of-use